

Timely reliable Bayesian decision-making enabled using memristors

Authors

Lekai Song¹, Pengyu Liu¹, Yang Liu^{1,2}, Jingfang Pei¹, Wenyu Cui³, Songwei Liu¹, Yingyi Wen¹, Teng Ma³, Kong-Pang Pun¹, Guohua Hu^{1,*}

Affiliations

¹Department of Electronic Engineering, The Chinese University of Hong Kong, Shatin, New Territories, Hong Kong S. A. R., China

²Shun Hing Institute of Advanced Engineering, The Chinese University of Hong Kong, Shatin, New Territories, Hong Kong S. A. R., China

³Department of Applied Physics, Hong Kong Polytechnic University, Hung Hom, Kowloon, Hong Kong S. A. R., China

*Correspondence to: ghhu@ee.cuhk.edu.hk

Abstract

Brains perform timely reliable decision-making by Bayes theorem. Bayes theorem quantifies events as probabilities and, through probability rules, renders the decisions. Learning from this, applying Bayes theorem in practical problems can visualize the potential risks and decision confidence, thereby enabling efficient user-scene interactions. However, given the probabilistic nature, implementing Bayes theorem with the conventional deterministic computing can inevitably induce excessive computational cost and decision latency. Herein, we propose a probabilistic computing approach using memristors to implement Bayes theorem. We integrate volatile memristors with Boolean logics and, by exploiting the volatile stochastic switching of the memristors, realize Boolean operations with statistical probabilities and correlations, key for enabling Bayes theorem. To practically demonstrate the effectiveness of our memristor-enabled Bayes theorem approach in user-scene interactions, we design lightweight Bayesian inference and fusion operators using our probabilistic logics and apply the operators in road scene parsing for self-driving, including route planning and obstacle detection. The results show that our operators can achieve reliable decisions at a rate over 2,500 frames per second, outperforming human decision-making and the existing driving assistance systems.

Main text

Brains are adept to make timely reliable decision-making for events with uncertainties. This ability is attributed to *Bayes theorem*, a mathematical principle used to determine the probability of an event to occur when given certain conditions (1). In Bayes theorem, all these events, conditions, and their relations are quantified as probabilities. This probabilistic data representation allows for probabilistic computation following the fundamental probability rules to render reliable decisions. Therefore, Bayes theorem shows promise in visualizing potential risks and decision confidence in enabling practical user-scene interactions (2, 3). However, given its probabilistic nature, efficiently implementing Bayes theorem remains challenging due to the lack of specialized hardware to deal with the probabilistic data representation and computation. Using the conventional deterministic binary computing systems for probabilistic data representation and computation, however, can result in excessive computational cost and decision latency (4).

Idealistic Bayes theorem implementation demands a probabilistic computing solution to realize probabilistic data representation and computation. One feasible approach is to encode the data into streams of random bits, termed *stochastic numbers*, where the probability of the bit 1s determines the values of the stochastic numbers (5). The stochastic numbers, when fed into standard Boolean logic gates, can undergo bitwise Boolean operations and yield reconstructed stochastic numbers as the computation results. The results follow the corresponding Boolean operations and, notably, probability rules. Given this probabilistic data representation and computation nature, the probabilistic Boolean operation enabled computing approach is well-suited to facilitate Bayes theorem implementation. Early electronic circuits based on *linear feedback shift registers* (LFSR) have demonstrated the ability for stochastic number encoding by employing the stochasticity inherent in the circuits (6–8). These circuits can also be conveniently integrated with Boolean logic gates to process the stochastic numbers conforming to probabilistic computing. However, these circuits typically entail intricate designs, resulting in considerable computational costs. Besides, correlations between the stochastic numbers are critical for the probabilistic Boolean operations, and an improper correlation from these circuits can corrupt the desired Boolean operations (9, 10).

To overcome the problems with the early circuits and realize timely reliable decision-making for user-scene interactions, here we propose a memristor-enabled probabilistic computing approach for Bayes theorem implementation. We integrate volatile memristors with standard Boolean logic gates and, by exploiting the volatile stochastic switching of the memristors, realize probabilistic data encoding and computation that are essential for Bayes theorem. Using the memristor-enabled probabilistic Boolean logics, we design lightweight Bayesian operators capable of performing two key Bayesian functions: inference and fusion. To demonstrate their effectiveness in practical user-scene interactions, we apply the operators in road scene parsing for self-driving, including route planning and obstacle detection. Our results show the operators can perform reliable decisions with a timeframe less than 0.4 ms (equivalently 2,500 fps), outperforming human decision-making and the advanced driver assistance systems. The results underpin the potential of our memristor-enabled probabilistic computing approach to realize Bayesian systems for user-scene interactions, for instance, self-driving, virtual reality, robotics, brain-machine interfaces, and beyond.

Volatile memristors

Memristors are resistive switching devices and they present a varying volatility depending on the switching mechanisms (11). Amongst them, volatile memristors switch with a self-reset threshold

behaviour (12). However, nonideal stochasticity tends to exhibit in the switching, for both volatile and non-volatile memristors, as a result of the underlying switching dynamics. For example, due to the stochastic diffusion of the conductive elements, filamentary memristors switch with a stochasticity (13). Given the self-reset threshold behaviour and, particularly, the adversary stochasticity, volatile memristors show promise to enable stochastic number encoding with no excessive hardware or computational cost (14–16).

Towards our proposed probabilistic computing approach for Bayes theorem implementation, we develop volatile filamentary memristors from solution-processed hexagonal boron nitride (hBN), following our previous report (17). We start with liquid-phase exfoliation of hBN, and then fabricate the memristors via photolithography in a Pt/Au/hBN/HfO_x/Ag structure (Fig. S1). Figure 1a shows an array of the memristors as fabricated. To assess the switching behaviour, we conduct sweeping tests on the memristors (Fig. 1b). In a typical switching, the memristor switches on to a low resistive state when the bias is over a threshold voltage V_{th} , and spontaneously resets to a high resistive state when the bias recedes below a hold voltage V_{hold} . This switching behaviour is governed by the underlying silver ion filamentary behaviour and, specifically, this exhibited volatility is due to the interplay between the bias and the Joule heat – a bias below V_{hold} cannot sustain the silver filaments due to the accompanying Joule heat (17). See also Fig. S2 for the ultrafast, ultralow power volatile switching of the memristors, with a switching time of ~50 ns, a relaxation time of ~1,100 ns, and a switching energy of ~0.16 nJ per bit.

As the sweeping test continues, the memristor exhibits stochasticity in the switching, with a consistent cycle-to-cycle stochasticity in V_{th} (2.08 ± 0.28 V) and V_{hold} (0.98 ± 0.30 V), well-fitting Gaussian distributions. The stochasticity arises from the underlying switching dynamics of the memristors, as the silver ion diffusion and filament formation/rupture are stochastic (13, 18, 19). To assess the stochasticity further, we perform a sampling test with 10 randomly selected devices from the array (Fig. S3). As demonstrated, all the 10 sampled devices exhibit a stable stochasticity in the switching. We plot the overall device-to-device stochasticity in Fig. 1c, with the distributions of the measured V_{hold} and V_{th} of the individual sampled memristors in Fig. 1d. The device-to-device stochasticity is ~8% in V_{th} , measured by the *coefficient of variation*, i.e., the ratio of the standard deviation to the mean of V_{th} in sampled memristors, proving a high device-to-device uniformity. Having confirmed the stable, uniform cycle-to-cycle and device-to-device stochastic switching, we perform Ornstein-Uhlenbeck process modelling on V_{th} (Fig. S4). The measured V_{th} of each of the sampled memristors follows a mean-reverting behaviour with random fluctuations, conforming to the Ornstein-Uhlenbeck process. Ornstein-Uhlenbeck process describes a stochastic process in a dynamical system (14). This indicates the stability of the switching stochasticity of our memristors in long-term switching operations. Indeed, pulsed cycling switching test proves a switching endurance of our memristors over 10^6 cycles (Fig. 1e).

The demonstrated stable volatile stochastic switching suggests that our memristors when exploited for probabilistic computing can allow for lightweight stochastic encoding of the input. The volatile switching can eliminate the need for peripheral circuits or excessive resetting operations for the switching operation, while the switching stochasticity can be harnessed for stochastic number encoding. On the other hand, importantly, the device-to-device uniformity can facilitate simplified device calibrations when several memristors are integrated to implement probabilistic computing.

Notably, the sampling test also suggests a high success rate of our memristor fabrication approach, with a yield approaching 100%, facilitating probabilistic computing implementation.

Probabilistic logics

Using our volatile memristors, we then design stochastic number encoders (SNEs) for stochastic encoding of the input with desired probabilities and correlations, to realize the probabilistic data representation as required for Bayes theorem implementation. In contrast to the early encoders that harness the stochasticity present in the electronic circuits (6–8), our proposed memristor-enabled SNEs exploiting the stochastic volatile switching can lead to simplified circuit designs.

As designed (Fig. 2a), the memristors are integrated with comparators to implement lightweight SNEs. See also Fig. S5 for the hardware implementation. When fed with pulsed signal V_{in} , the memristors are switched stochastically, and the output from the memristors carrying the stochasticity is binarized by the comparators via the reference V_{ref} . This then yields stochastic numbers with probabilities, and the probabilities can be well-regulated by V_{in} and V_{ref} . Notably, as designed, the stochastic numbers from a SNE are correlated, while the stochastic numbers from two or more parallel SNEs are uncorrelated. Figure 2b presents the probability of uncorrelated stochastic numbers $P_{uncorrelated}$ with respect to V_{in} . As V_{in} increases, $P_{uncorrelated}$ is increased, as the memristors tend to be switched on with a higher probability. This relation follows a sigmoidal fit, proving that V_{in} can effectively regulate $P_{uncorrelated}$. Similarly, Fig. 2c presents the probability of correlated stochastic numbers $P_{correlated}$ with respect to V_{ref} . In this case, $P_{correlated}$ is decreased as V_{ref} increases, as V_{ref} serves as the threshold for binarization. This relation also follows a sigmoidal fit, proving that V_{ref} can also effectively regulate $P_{correlated}$. Therefore, as demonstrated, our SNEs can perform stochastic number encoding with desired and well-regulated probabilities and correlations. This suggests that our SNEs can facilitate convenient integration with Boolean logic gates for performing probabilistic computing.

As examples, here we show the integration of our SNEs with standard Boolean logic gates to build probabilistic AND and MUX logics in uncorrelation, as they can conduct key Boolean operations in Bayes theorem (Fig. 2d). For probabilistic AND logic, two parallel SNEs are connected to a AND gate, and the uncorrelated stochastic number outputs from the SNEs serve as the inputs to the AND gate. Upon operation, based on the $P_{uncorrelated}-V_{in}$ relation in Fig. 2b, the SNEs when fed with pulsed signals of the corresponding V_{in} output uncorrelated stochastic numbers, denoted as a and b , with probabilities of $P(a)$ and $P(b)$, respectively. Then, a and b are bit-by-bit fed into the AND gate, outputting a stochastic number, denoted as c , with a probability of $P(c)$. We show in Fig. 2e the corresponding stochastic numbers and probabilities from the hardware test. The statistical relation, i.e., $P(a)P(b) \approx P(c)$, proves that the probabilistic AND logic successfully functions as a multiplier to conduct one-step multiplication of stochastic numbers. Here we note that, compared to conventional binary multipliers, our probabilistic AND logic not only simplifies the circuit design but also reduces the computational cost. The probabilistic AND logic can also be configured in correlation. In this case, SNEs are configured to output correlated stochastic numbers according to the $P_{correlated}-V_{in}$ relation in Fig. 2c, and the probabilistic AND logic outputs the minimum of the inputs i.e., $P(c) \approx \min(P(a), P(b))$ (Fig. 2e). Similarly, we design probabilistic MUX logic in both uncorrelation and correlation configurations and perform their one-step weighted addition operations (Fig. 2e). Here the select and inputs of the probabilistic MUX logics must be uncorrelated to perform the operations properly (Fig. S6). We present in

Table S1 a summary of the probabilistic logics including AND, OR, XOR, and MUX logics in the varying correlations.

The probabilistic logics with the desired probabilities and correlations can potentially be integrated to enable probabilistic computing towards Bayes theorem implementation. Note that in the above demonstrations the stochastic numbers are all encoded in 100-bit for illustrative purposes. A longer bit length renders a higher precision in data representation, however, with a higher computational cost. The bit length can be adjusted to accommodate tasks with the different precision requirements, given the trade-off between the computational cost and precision.

Bayesian inference

To instantiate Bayes theorem, we apply our memristor-enabled probabilistic logics to implement Bayesian inference, a reliable decision-making method. Inference is a process of drawing conclusions based on the known facts. Despite being investigated in multiple disciplines including logic, neuroscience, cognitive psychology, and computer science (20–22), the essence of inference remains elusive, let alone its implementation via lightweight probabilistic computing. Nevertheless, Bayes theorem provides a probabilistic perspective to explain and achieve inference (23). In Bayesian inference, the term *prior knowledge* is used to denote the known facts, while *belief* the confidence (or reliability) of a certain decision. Importantly, as all the prior knowledge and beliefs can be quantified as probabilities, Bayesian inference can effectively revise the prior knowledge with new information, using the rules of probability, to make reliable decisions.

As we demonstrate, our memristor-enabled probabilistic logics are well capable of performing probabilistic data representation and computation, conforming to Bayesian inference. Herein, we design a hardware Bayesian operator using our memristor-enabled probabilistic logics to perform Bayesian inference (Fig. 3a; see also Fig. S7 for the hardware implementation), following the Bayesian inference theorem:

$$P(A|B) = \frac{P(A)P(B|A)}{P(B)} = \frac{P(A)P(B|A)}{P(A)P(B|A) + P(\neg A)P(B|\neg A)}. \quad (1)$$

As designed, our memristor-enabled probabilistic AND and MUX logics are used to conduct the one-step multiplication and weighted addition operations, respectively, for functioning as the numerator and denominator of the equation (1). The division itself is achieved using a probabilistic MUX plus a D-Flip-Flop, following a classic divider design for stochastic numbers, CORDIV (24). When in operation to perform Bayesian inference, the prior knowledge with a prior probability $P(A)$ is updated when the new information with a marginal probability $P(B)$ is available, to yield a reliable decision with a posterior probability $P(A|B)$.

To investigate the effectiveness of our Bayesian inference operator in practical applications, we apply the operator in route planning for self-driving. Route planning for self-driving has been a challenging topic, demanding great efforts to deal with the complex traffic conditions, the vehicle driving, and the lane-changing situations. Particularly, given that any delay in the decision making can lead to severe traffic accidents, achieving timely reliable decisions is critical for route planning. Bayesian inference has been conventionally commonly adopted in route planning for self-driving (25), as it can help make safe, reliable decisions by combining the prior knowledge (e.g. the traffic rules, road structure, and driving behaviours) and the latest lane information (e.g. the obstacles, accidents, and weather conditions). However, as discussed, the conventional approaches can incur

excessive computational cost and, particularly, decision latency (4). Figure 3a illustrates our Bayesian operator in route planning. For example, when a vehicle (coloured in red) tries to change its lane, it may evaluate the situation in the target lane through Bayesian inference to determine whether to cut in the target lane or not. Bayesian inference takes the latest lane information $P(B)$ into account and updates the prior probability $P(A)$ to achieve a posterior probability $P(A|B)$. If $P(A|B)$ exceeds $P(A)$, indicating a high possibility for a safe lane change, the vehicle may cut in the lane. Otherwise, the vehicle may maintain its current lane.

Figure 3b presents the hardware test results of our Bayesian inference operator in route planning. Specially, the prior probability $P(A)$ represents the initial belief of the vehicle of investigation (coloured in red) to try to cut in the lane, considering the prior knowledge only. The marginal probability $P(B)$ represents the probability when the vehicle spots another vehicle (coloured in blue) on the target lane, i.e., the latest lane information. The posterior probability $P(A|B)$ reflects the updated belief of the vehicle after considering $P(A)$ and $P(B)$ using the Bayesian inference theorem. For illustrative purposes, $P(A) = 57\%$ and $P(B) = 72\%$ are manually set to initialize the Bayesian inference operator. As demonstrated, the operator integrates the prior knowledge with the latest lane information to make a final decision with a probability $P(A|B) = 63\%$. This probability aligns with the theoretical result in the equation (1), $\sim 61\%$, validating the effectiveness of our Bayesian inference operator in performing Bayesian inference. Based on the, the vehicle can make lane-changing decision with a higher confidence. This enhanced decision reliability is attributed to the comprehensive evaluation via our Bayesian inference operator for both the vehicle itself and traffic situation. We emphasize that the enhanced decision reliability is irrespective of the exact values of $P(A|B)$ and $P(A)$. For example, even if $P(A) > P(A|B)$, the operator can still make a reliable decision, i.e., maintaining its current lane.

Note that, to make our Bayesian inference operator lightweight for timely decision-making, we maximize the sharing of the SNEs in the circuit design. This is done under the condition that the strict regulation over the probabilities and correlations of the stochastic numbers ensures the proper functions of the Multiplier, Adder, and Divider. To clarify, we quantify the pairwise correlations between the stochastic numbers involved in the Bayesian inference using *Pearson correlation* and *SC correlation* (Fig. 3c and d). The results confirm that all the probabilistic logics in the operator work in the desired correlations and, as such, conduct the corresponding Boolean operations for performing Bayesian inference. Though the above demonstration studies the case where the decision-making is affected by one variable only (denoted as the one-parent-one-child, i.e. $A \rightarrow B$), our Bayesian inference operator can be readily generalized to more complicated cases, for instance, two-parent-one-child ($A_1 \rightarrow B \leftarrow A_2$), and one-parent-two-child ($B_1 \leftarrow A \rightarrow B_2$) (Fig. S8). In addition, arising from the ultrafast switching of the memristors ($\sim 4 \mu\text{s}$ per bit, Fig. S2), our Bayesian inference operator with 100-bit stochastic number encoding can achieve Bayes inference with a time-frame of 0.4 ms per frame, i.e., 2,500 fps. Note that here we neglect the delays of the comparators and Boolean logic gates, as the switching of memristors (though ultrafast) is still the bottleneck of the operator. In this consideration, our Bayesian inference operator outperforms human decision-making (0.7-1.5 ms reaction time (26)) and the advanced driver assistance systems (30-45 fps (27)) in route planning.

Bayesian fusion

Besides inference, fusion is another key Bayesian decision-making approach. While inference integrates the past and present information, fusion integrates information from multiple modalities. Given that each modality only represents a fragment of information, Bayesian fusion aims to integrate the multimodal information to address the single-modal shortages and as such, achieve more reliable decisions (20). Similar to Bayesian inference, all the information in Bayesian fusion is represented and computed by probabilities. Herein we investigate the potential of our memristor-enabled probabilistic logics in implementing Bayesian multimodal fusion. We reconfigure the circuits to design a hardware Bayesian fusion operator, as shown in Fig. 4a. See also S9 for the detailed circuit design and hardware implementation.

To investigate the effectiveness of our Bayesian fusion operator in practical applications, we apply the operator in obstacle detection in low-visibility self-driving scenarios. Here we take a self-driving vehicle equipped with RGB and thermal cameras as the example. A RGB camera is commonly used to extract obstacle signatures in self-driving, but this requires a good visibility. On the contrary, a thermal camera works almost for any visibility conditions, but it can only detect obstacles with heat emission. In this context, decision-making based on a single-modal information from either a RGB camera or a thermal camera tends to be unreliable, particularly, in low-visibility conditions. To address this problem, RGB-thermal Bayesian fusion has been previously proposed as a promising solution for reliable decision-making in various low-visibility conditions, including nighttime, rain, and fog (2, 3). Nevertheless, as discussed, implementing Bayesian fusion using the conventional approaches can incur excessive computational cost and decision latency (4).

Here we apply our Bayesian fusion operator in obstacle detection as outlined in Fig. 4a. Pre-trained edge neural networks tailored for processing RGB and thermal information output single-modal obstacle detection decisions, denoted as $P(y|x_1)$ and $P(y|x_2)$, where y represents the detected obstacle, and x_1 and x_2 the RGB and thermal input, respectively. The Bayesian fusion operator fuses the single-modal RGB and thermal decisions into a decision $p(y|x_1, x_2)$, following,

$$p(y|x_1, x_2) = \frac{p(x_1, x_2|y)p(y)}{p(x_1, x_2)} \propto p(x_1, x_2|y)p(y) \quad (2)$$

Assuming x_1 and x_2 are conditionally independent with given y , we have,

$$p(x_1, x_2|y) = p(x_1|y)p(x_2|y) \quad (3)$$

Substituting the equation (3) into (2), we get,

$$p(y|x_1, x_2) \propto p(x_1|y)p(x_2|y)p(y) = \frac{p(x_1|y)p(y)p(x_2|y)p(y)}{p(y)} \propto \frac{p(y|x_1)p(y|x_2)}{p(y)} \quad (4)$$

That is, our Bayesian multimodal fusion is implemented by multiplying two preliminary single-modal decisions and then divided by the prior probability of obstacles (28). Considering that the output probability may exceed one, we integrate a normalization module to ensure reliable and reasonable output probability as the final multimodal fusion decision (Fig. S10).

We test our Bayesian fusion operator with real self-driving dataset, *FLIR* (29). The dataset consists of aligned RGB-thermal image pairs captured under different visibility conditions during daytime and nighttime. The dataset is respectively processed by the pre-trained neural networks, denoted as RGB-only and thermal-only networks, to output preliminary single-modal decisions. The single-modal RGB and thermal decisions serve as the inputs to our Bayesian fusion operator to yield obstacle detection results, as presented in Fig. 4b. As demonstrated, before fusion, the thermal-only network loses certain target obstacles. This may be ascribed to the distance between

the obstacles and the thermal camera, and the insufficient thermal emissions from the obstacles. The RGB-only network also misses certain target obstacles, particularly during low-visibility nighttime. Besides, though the two single-modal networks are capable of detecting obstacles, they sometimes fail to provide confident decisions. Our Bayesian fusion operator is proved effective to address these issues. On the one hand, our operator can integrate the preliminary single-modal decisions to generate a final decision, resolving the issue of target missing. On the other hand, our operator can make more confident decisions by leveraging the Bayesian fusion theorem.

Similar to our Bayesian inference operator, our Bayesian fusion operator also maximizes the sharing of the SNEs and makes well use of the correlations to realize lightweight circuit design. Besides, equation (4) can be easily generalized to allow more modality fusion beyond two by,

$$p(y|x_1, x_2 \cdots x_M) = \frac{\prod_{i=1}^M p(y|x_i)}{p(y)^{M-1}} \quad (5)$$

In addition, similarly, arising from the ultrafast switching of the memristors, the operator with 100-bit stochastic number encoding can easily achieve Bayesian fusion with 2,500 fps. Considering the sampling rate of the cameras (10-30 fps, (30)) and the processing speed of the pre-trained networks (300 fps, (31)) deployed in real-world self-driving, our operator is a promising timely reliable obstacle detection solution for self-driving.

Conclusion

We have implemented timely reliable Bayes decision-making using probabilistic Boolean logics enabled with memristors. The probabilistic logics, employing the volatile stochastic switching of the memristors, allow for probabilistic data representation and Boolean operations to facilitate Bayes theorem computing. As practical demonstration of our memristor-enabled Bayes decision-making in user-scene interactions, we realize lightweight Bayesian inference and fusion operators with the probabilistic logics, and prove their remarkable performance in in road scene parsing for self-driving, including route planning and obstacle detection, outperforming human decision-making and the advanced driving assistance systems. Given this remarkable performance and the compacity of the circuit designs, as well as the scalability of our memristors, our probabilistic logics are readily scaled-up and generalised towards the development of Bayesian systems for real-world user-scene interactions. As demonstrated, arising from the ultrafast switching of the memristors, a large-scale probabilistic logic circuit with 100-bit stochastic number encoding can easily achieve user-scene interactions with a frame rate of 2,500 fps, fulfilling the requirements of widespread applications including self-driving, virtual reality, robotics, brain-machine interfaces, and beyond.

Methods

Memristors: Pristine hBN powder and all chemicals are purchased from Sigma-Aldrich and used as received. Liquid-phase exfoliation, ink formulation, and deposition of hBN follow our method previously reported in Ref. (17). In a typical process (Fig. S1), the memristor is fabricated in a vertical Pt/Au/hBN/HfO_x/Ag configuration, where hBN is deposited by slot-die coating, the HfO_x layer (20 nm) is deposited by atomic layer deposition, and the metal electrodes (5/15 nm Pt/Au and 30 nm Ag) are patterned by photolithography and deposited by electron beam evaporation. During device fabrication, the hBN layer after deposition is baked at 200°C for 2 hours.

Stochastic number encoders and probabilistic logics: To build the SNEs and probabilistic logics, the memristors are tested on a probe station and connected to the logic gates and other electronic devices on a breadboard. Tektronix Keithley 4200A-SCS parameter analyser with pulse measure units is used to measure the electrical characteristics of the memristors. Siglent arbitrary waveform generators and digital storage oscilloscopes are used to output signals and measure waveforms. To endow the stochastic numbers with a certain probability, based on the $P_{\text{uncorrelated}}-V_{\text{in}}$ and $P_{\text{correlated}}-V_{\text{in}}$ relations in Fig. 2b and c, each stochastic number encoder is fed with n -cycle pulsed signals of the corresponding V_{in} to encode n -bit stochastic numbers.

Stochastic number correlation: The correlation between the stochastic numbers S_x and S_y is quantified using the *Pearson correlation* (ρ) and *SC correlation* (SCC) (9), following,

$$\rho(S_x, S_y) = \frac{ad - bc}{\sqrt{(a+b)(a+c)(b+d)(c+d)}}$$

and

$$SCC(S_x, S_y) = \begin{cases} \frac{ad - bc}{(a+b+c+d) \min(a+b, a+c) - (a+b)(a+c)}, & ad \geq bc \\ \frac{ad - bc}{(a+b)(a+c) - (a+b+c+d) \max(a-d, 0)}, & ad < bc \end{cases}$$

where a , b , c , and d represent the counts of 1-1, 1-0, 0-1, and 0-0 pairs of two stochastic numbers S_x and S_y , respectively.

Bayesian fusion: The pre-trained RGB-only and thermal-only networks used are the *Ultralytics YOLOv8n* (32) and *Roboflow flir-data-set/22* (29), respectively. The prior of the obstacle $p(y)$ is assumed to be uniform for the convenience of circuit designs. Limited by the scalability of the lab-based realisation of the hardware Bayesian operator, Bayesian fusion is conducted on multimodal fusion of individual images only. Large-scale Bayesian fusion that is implementable with large-scale hardware Bayesian operator circuits is conducted via simulation in Python for processing high-speed streaming videos.

References

1. D. C. Knill, A. Pouget, The Bayesian brain: The role of uncertainty in neural coding and computation. *Trends in Neurosciences* **27**, 712–719 (2004).
2. W. Zhou, X. Lin, J. Lei, L. Yu, J. N. Hwang, MFFENet: multiscale feature fusion and enhancement network for RGB-thermal urban road scene parsing. *IEEE Transactions on Multimedia* **24**, 2526–2538 (2022).
3. Y. Sun, W. Zuo, P. Yun, H. Wang, M. Liu, FuseSeg: semantic segmentation of urban scenes based on RGB and thermal data fusion. *IEEE Transactions on Automation Science and Engineering* **18**, 1000–1011 (2021).
4. D. Bonnet, T. Hirtzlin, A. Majumdar, T. Dalgaty, E. Esmanhotto, V. Meli, N. Castellani, S. Martin, J.-F. Nodin, G. Bourgeois, J.-M. Portal, D. Querlioz, E. Vianello, Bringing uncertainty quantification to the extreme-edge with memristor-based Bayesian neural networks. *Nature Communications* **14**, 7530 (2023).
5. A. Alaghi, W. Qian, J. P. Hayes, The promise and challenge of stochastic computing. *IEEE Transactions on Computer-Aided Design of Integrated Circuits and Systems* **37**, 1515–1531 (2018).
6. P. Knag, W. Lu, Z. Zhang, A native stochastic computing architecture enabled by memristors. *IEEE Transactions on Nanotechnology* **13**, 283–293 (2014).
7. S. Gaba, P. Sheridan, J. Zhou, S. Choi, W. Lu, Stochastic memristive devices for computing and neuromorphic applications. *Nanoscale* **5**, 5872–5878 (2013).
8. S. A. Salehi, Low-Cost Stochastic Number Generators for Stochastic Computing. *IEEE Transactions on Very Large Scale Integration (VLSI) Systems* **28**, 992–1001 (2020).
9. A. Alaghi, J. P. Hayes, Exploiting correlation in stochastic circuit design. *2013 IEEE 31st International Conference on Computer Design, ICCD 2013*, 39–46 (2013).
10. H. Ichihara, S. Ishii, D. Sunamori, T. Iwagaki, T. Inoue, Compact and accurate stochastic circuits with shared random number sources. *2014 32nd IEEE International Conference on Computer Design, ICCD 2014*, 361–366 (2014).
11. L. O. Chua, Memristors on ‘edge of chaos.’ *Nature Reviews Electrical Engineering* **1** (2024).
12. S. Kumar, X. Wang, J. P. Strachan, Y. Yang, W. D. Lu, Dynamical memristors for higher-complexity neuromorphic computing. *Nature Reviews Materials* **7**, 575–591 (2022).
13. J. Tang, F. Yuan, X. Shen, Z. Wang, M. Rao, Y. He, Y. Sun, X. Li, W. Zhang, Y. Li, B. Gao, H. Qian, G. Bi, S. Song, J. J. Yang, H. Wu, Bridging Biological and Artificial Neural Networks with Emerging Neuromorphic Devices: Fundamentals, Progress, and Challenges. *Advanced Materials* **31**, e1902761 (2019).
14. S. Dutta, G. Detorakis, A. Khanna, B. Grisafe, E. Neftci, S. Datta, Neural sampling machine with stochastic synapse allows brain-like learning and inference. *Nature Communications* **13**, 2571 (2022).
15. W. A. Borders, A. Z. Pervaiz, S. Fukami, K. Y. Camsari, H. Ohno, S. Datta, Integer factorization using stochastic magnetic tunnel junctions. *Nature* **573**, 390–393 (2019).
16. Q. Xia, J. J. Yang, Memristive crossbar arrays for brain-inspired computing. *Nature Materials* **18**, 309–323 (2019).
17. L. Song, P. Liu, J. Pei, F. Bai, Y. Liu, S. Liu, Y. Wen, L. W. T. Ng, K. P. Pun, S. Gao, M. Q. H. Meng, T. Hasan, G. Hu, Spiking neurons with neural dynamics implemented using stochastic memristors. *Advanced Electronic Materials* **2300564**, 1–9 (2023).
18. Z. Wang, S. Joshi, S. E. Savel’ev, H. Jiang, R. Midya, P. Lin, M. Hu, N. Ge, J. P. Strachan, Z. Li, Q. Wu, M. Barnell, G. L. Li, H. L. Xin, R. S. Williams, Q. Xia, J. J. Yang, Memristors

- with diffusive dynamics as synaptic emulators for neuromorphic computing. *Nature Materials* **16**, 101–108 (2017).
19. C. P. Hsiung, H. W. Liao, J. Y. Gan, T. B. Wu, J. C. Hwang, F. Chen, M. J. Tsai, Formation and instability of silver nanofilament in Ag-based programmable metallization cells. *ACS Nano* **4**, 5414–5420 (2010).
 20. U. Noppeney, Perceptual Inference, Learning, and Attention in a Multisensory World. *Annual Review of Neuroscience* **44**, 449–473 (2021).
 21. T. Rohe, A. C. Ehrlis, U. Noppeney, The neural dynamics of hierarchical Bayesian causal inference in multisensory perception. *Nature Communications* **10**, 1–17 (2019).
 22. Y. Lecun, Y. Bengio, G. Hinton, Deep learning. *Nature* **521**, 436–444 (2015).
 23. R. van de Schoot, S. Depaoli, R. King, B. Kramer, K. Märtens, M. G. Tadesse, M. Vannucci, A. Gelman, D. Veen, J. Willemsen, C. Yau, Bayesian statistics and modelling. *Nature Reviews Methods Primers* **1** (2021).
 24. T. H. Chen, J. P. Hayes, Design of division circuits for stochastic computing. *Proceedings of IEEE Computer Society Annual Symposium on VLSI, ISVLSI 2016-Septe*, 116–121 (2016).
 25. K. Wang, Y. Wang, B. Liu, J. Chen, Quantification of Uncertainty and Its Applications to Complex Domain for Autonomous Vehicles Perception System. *IEEE Transactions on Instrumentation and Measurement* **72**, 1–17 (2023).
 26. M. Green, “How Long Does It Take to Stop?” Methodological Analysis of Driver Perception-Brake Times. *Transportation Human Factors* **2**, 195–216 (2000).
 27. D. Gehrig, D. Scaramuzza, Low-latency automotive vision with event cameras. *Nature* **629**, 1034–1040 (2024).
 28. Y.-T. Chen, J. Shi, Z. Ye, C. Mertz, D. Ramanan, S. Kong, “Multimodal Object Detection via Probabilistic Ensembling” in *Computer Vision -- ECCV 2022*, S. Avidan, G. Brostow, M. Cissé, G. M. Farinella, T. Hassner, Eds. (Springer Nature Switzerland, Cham, 2022), pp. 139–158.
 29. T. Imaging, FLIR data set Dataset, *Roboflow Universe* (2024). <https://universe.roboflow.com/thermal-imaging-0hwfw/flir-data-set>.
 30. D. J. Yeong, G. Velasco-hernandez, J. Barry, J. Walsh, Sensor and sensor fusion technology in autonomous vehicles: A review. *Sensors* **21**, 1–37 (2021).
 31. H. Wang, C. Liu, Y. Cai, L. Chen, Y. Li, YOLOv8-QSD: An Improved Small Object Detection Algorithm for Autonomous Vehicles Based on YOLOv8. *IEEE Transactions on Instrumentation and Measurement* **73**, 1–16 (2024).
 32. G. Jocher, J. Qiu, A. Chaurasia, Ultralytics YOLO, version 8.0.0 (2023); <https://github.com/ultralytics/ultralytics>.

Acknowledgements

Funding: GH acknowledges support from CUHK (4055227) and RGC (24200521), YL from SHIAE (RNE-p3-21), JP and YW from RGC (24200521), TM from RGC (15306824) and ITC (ITS/150/23FP).

Author contributions: LS, PL, GH designed the experiments. LS, PL, YL, JP, WC, SL, YW performed the experiments. LS, GH analysed the data. LS, GH prepared the figures. LS, GH wrote the manuscript. All authors discussed the results from the experiments and commented on the manuscript.

Competing interests: The authors declare no competing financial interests.

Data and materials availability: The data that support the findings of this study are available from the corresponding authors upon request.

Figures

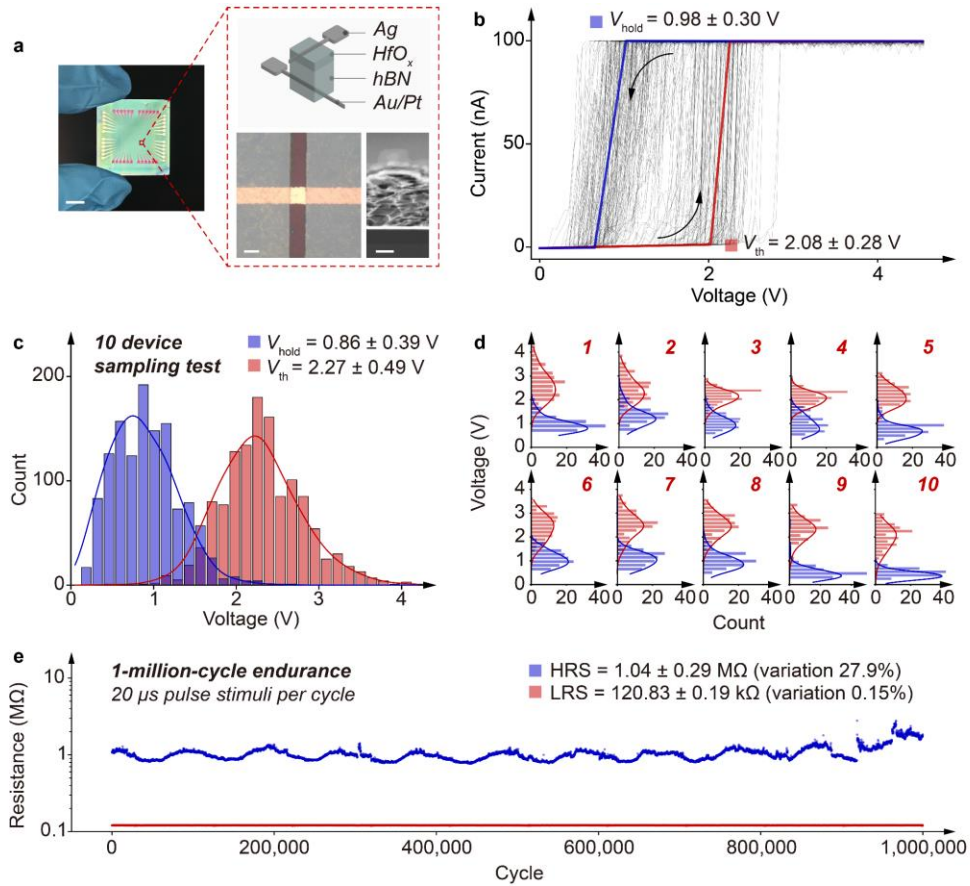


Figure 1. Volatile switching memristors. (a) 12×12 hBN memristors in a crossbar configuration, and the optical microscopic and cross-sectional transmission electron microscopic images of a typical memristor. Device area $\sim 20 \times 20 \mu\text{m}^2$. Scale bars – 5 μm , 20 μm , and 100 nm. (b) Current-voltage output from a typical memristor, showing 128-cycle stochastic yet stable switching with a switching ratio of $\sim 10^5$. A compliance current of 100 nA is set.

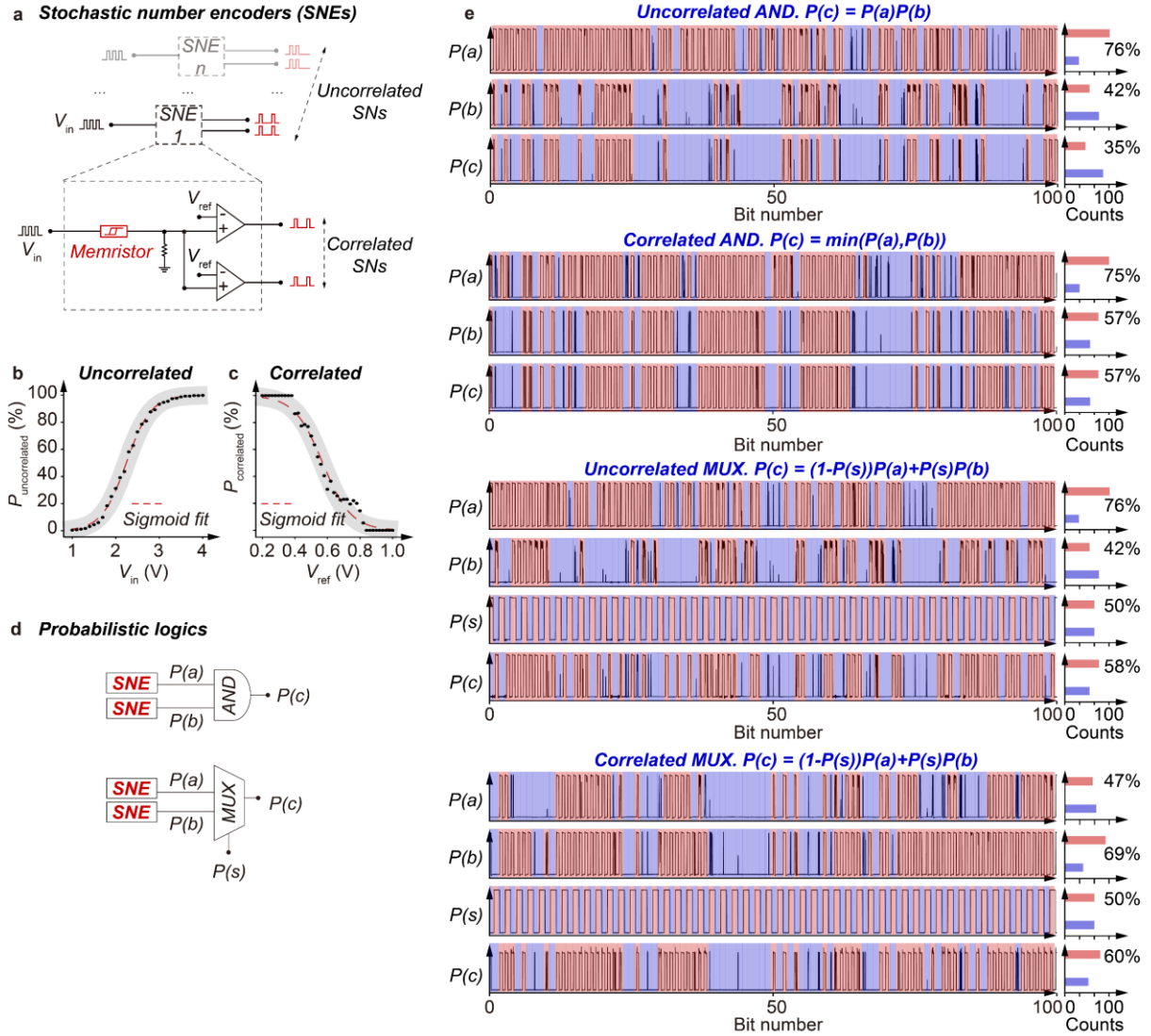


Figure 2. Memristor-enabled probabilistic logics. (a) Stochastic number encoders (SNEs), consisting of a memristor and a set of comparators. The output probability and correlation are regulated by the input V_{in} and reference V_{ref} . A SNE via circuit designs can output correlated stochastic numbers, while two or more parallel SNEs can output uncorrelated stochastic numbers. (b) $P_{\text{uncorrelated}}-V_{\text{in}}$ and (c) $P_{\text{correlated}}-V_{\text{ref}}$ relations of the SNEs in uncorrelation and correlation, well fitting sigmoid functions $P_{\text{uncorrelated}} = 1/(1 + \exp[-3.56(V_{\text{in}} - 2.24)])$ and $P_{\text{correlated}} = 1 - 1/(1 + \exp[-11.5(V_{\text{ref}} - 0.57)])$. (d) Probabilistic AND and MUX logics in uncorrelation, implemented with the SNEs and standard AND and MUX logics. The circuits can be reconfigured to implement other probabilistic logics and accommodate varying correlations. (e) Hardware tests of the probabilistic logics in (d) in both uncorrelation and correlation. Bit 0s and 1s are marked in blue and red. For probabilistic MUX, the frequency of select s is half of the inputs to ensure both the inputs participate in the logic operations. The outputs of the probabilistic logics in uncorrelation and correlation are consistent with the statistical relations in Table S1.

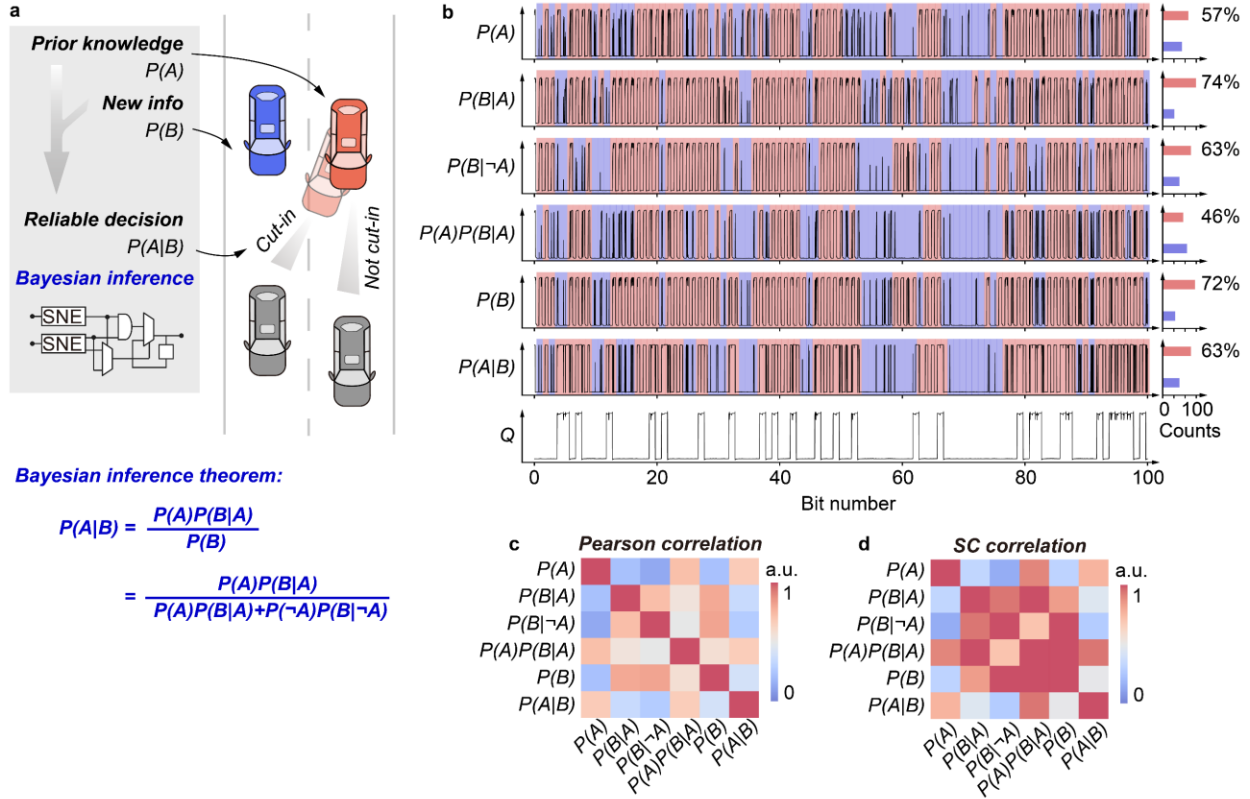


Figure 3. Bayesian inference. (a) Memristor-enabled Bayesian inference operator and its workflow to perform Bayesian inference for route planning. Prior knowledge with a prior probability $P(A)$ is updated as the new information with probability $P(B)$ becomes available, yielding a reliable decision with a posterior probability $P(A|B)$. Here $P(A)$ represents the initial belief of a vehicle (coloured in red) trying to cut in lanes, and $P(B)$ represents the probability of the vehicle spotting another vehicle (coloured in blue) on the target lane. The Bayesian inference operator is implemented with the memristor-enabled probabilistic AND and MUX logics. The probabilistic logics are used to conduct multiplication and weighted addition operations respectively for functioning as the numerator and denominator conforming to the Bayesian inference theorem. The division is achieved with a probabilistic MUX plus a D-Flip-Flop, following a classic divider design for stochastic numbers, CORDIV (24). See Fig. S7 for the detailed circuit design and hardware implementation. (b) Hardware test of the Bayesian inference operator to perform route planning for self-driving vehicles. $P(A)$ and $P(B)$ are manually set to initialize the operator. Stochastic numbers at the key nodes are plotted accordingly. Bit 0s and 1s are marked in blue and red. The result $P(A|B) > P(A)$ means the red vehicle in (a) can cut in lanes with higher confidence. This enhanced decision reliability is attributed to the comprehensive evaluation of both the vehicle itself and the traffic situation. Pairwise (c) Pearson and (d) SC correlations between the stochastic numbers in (b).

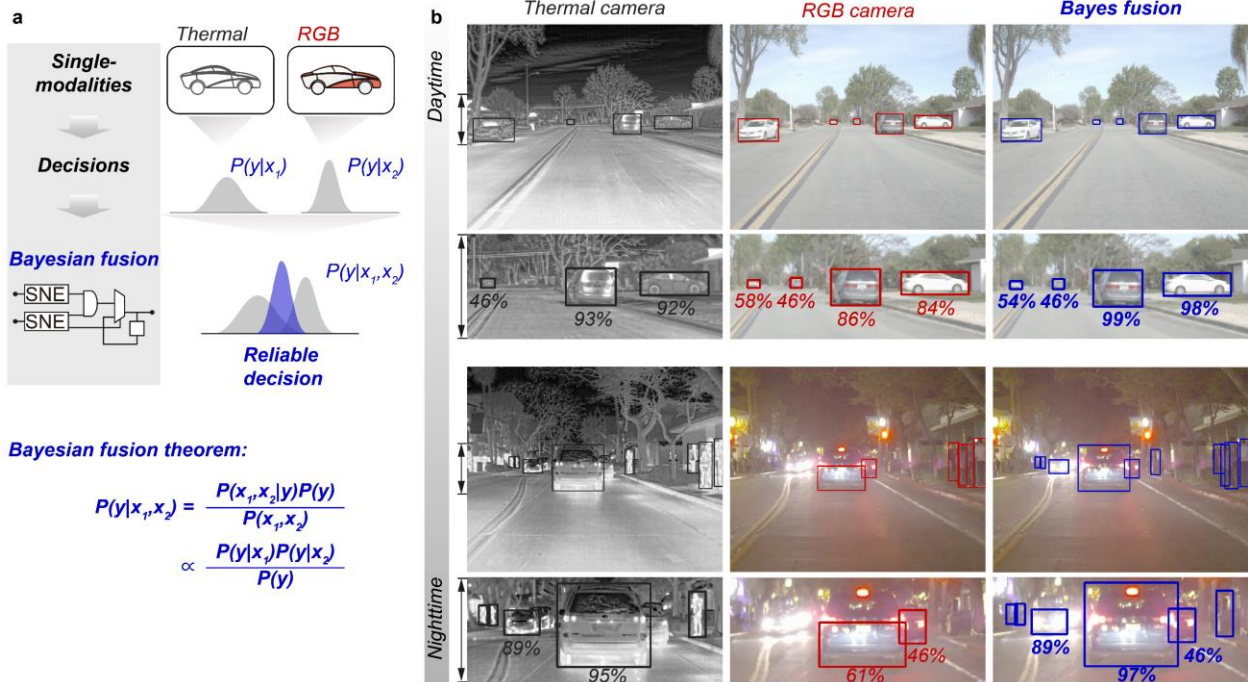


Figure 4. Bayesian fusion. (a) Memristor-enabled Bayesian fusion operator and its workflow to perform Bayesian fusion. Pre-trained neural networks tailored for single modalities receive RGB and thermal information and output single-modal obstacle detection decisions, denoted as $P(y|x_1)$ and $P(y|x_2)$, where y represents the detected obstacle, and x_1 and x_2 represent the RGB and thermal information, respectively. The Bayesian fusion operator fuses the single-modal decisions into a reliable decision, denoted as $p(y|x_1, x_2)$, using the Bayesian fusion theorem. The Bayesian fusion operator is implemented with the memristor-enabled probabilistic AND and MUX logics. The probabilistic logics are used to conduct multiplication and weighted addition operations respectively for functioning as the numerator and denominator conforming to the Bayesian fusion theorem. The division is achieved with a probabilistic MUX plus a D-Flip-Flop, following a classic divider design for stochastic numbers, CORDIV (24). See Fig. S9 for the detailed circuit design and hardware implementation. (b) Obstacle detection results before and after the Bayesian fusion of the RGB and thermal information under the different visibility conditions during daytime and nighttime. Before fusion, single-modal (RGB or thermal) networks typically lose certain target obstacles and make decisions with insufficient confidence. The Bayesian fusion operator effectively overcomes the single-modal shortages, addresses the target-missing and low-confidence issues, and achieves much accurate and reliable results.

Supplementary Figures

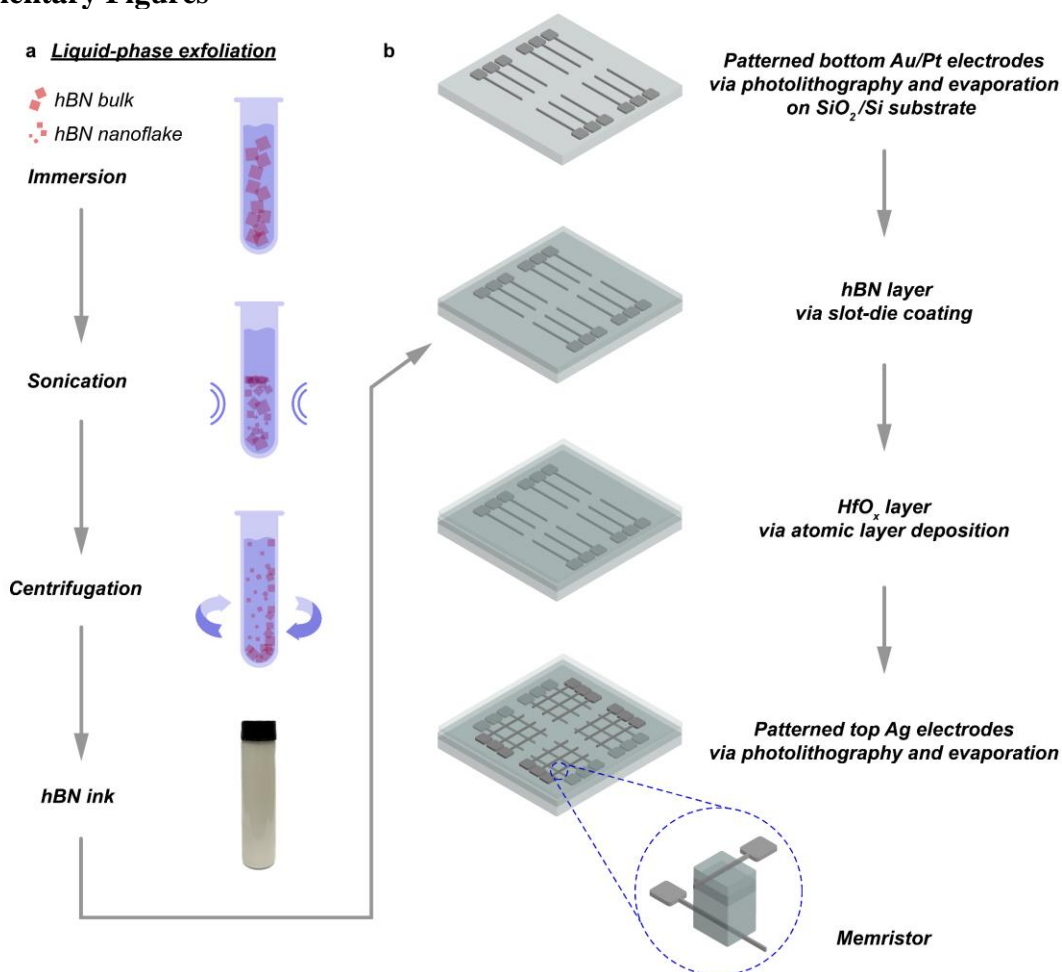


Figure S1. Memristor fabrication. (a) Schematic liquid-phase exfoliation of hBN, following our previous report (1). After 48-hour bath sonication, the dispersion of the as-exfoliated hBN nanoflakes in isopropanol is centrifuged at 4,000 rpm for 30 minutes (initial concentration of hBN ~ 10 mg/ml). The supernatant is then carefully decanted, collected, and added with controlled volumes of isopropanol and 2-butanol to formulate an ink in isopropanol/2-butanol (90 vol.%/10 vol.%) with a concentration of ~ 1 mg/ml. (b) Schematic device fabrication. Starting from a cleansed SiO₂/Si substrate, bottom Au/Pt electrodes are deposited and patterned by evaporation and photolithography. hBN layer is deposited on the bottom electrodes by slot-die coating the hBN ink as prepared. HfO_x layer (20 nm) is then deposited using atomic layer deposition to minimize the wash-off of hBN during the subsequent patterning process and increase the fabrication yield to $\sim 100\%$, while preserving the switching behavior of the filamentary memristors. Next, top silver electrodes are patterned by evaporation and photolithography. As schematically illustrated, the memristors are developed at the cross-points between the top and bottom metal electrodes, in a vertical Au/Pt/hBN/HfO_x/Ag device structure.

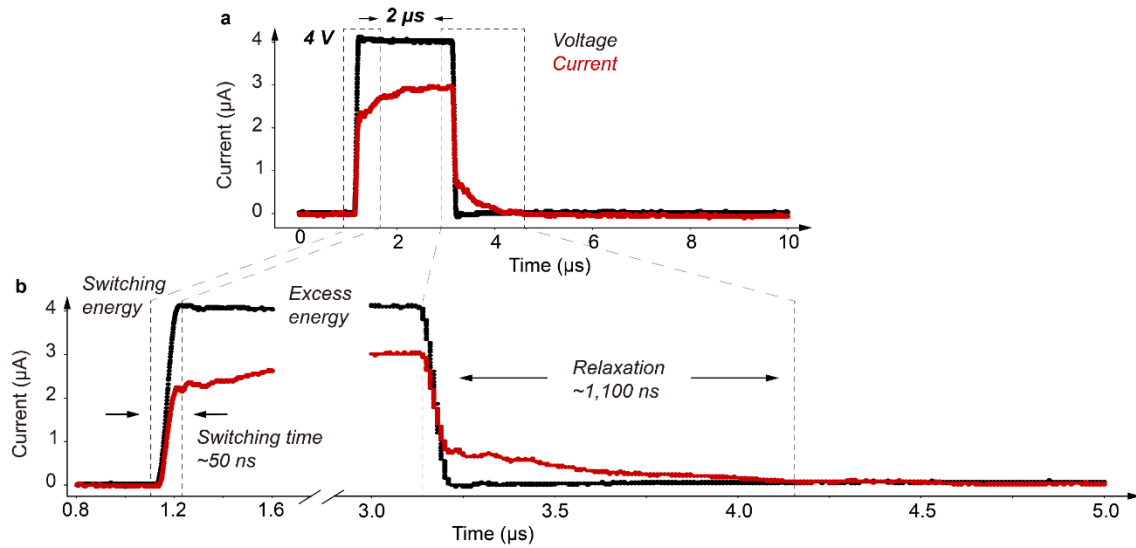


Figure S2. Switching speed and energy consumption of a typical memristor device. (a) Electrical response of a typical hBN memristor device to 2 µs pulsed signal, showing (b) a switching time of ~50 ns, a switching energy consumption of ~0.16 nJ, and a relaxation time of ~1,100 ns. Given that the entire switching process involves Joule heat, the energy consumption can be segregated into a switching energy and an excess energy (2). The switching energy is contributed to the resistive switching process, while the excess energy is contributed to the energy dissipation following the switching process. The switching energy can be estimated by integrating the product of the transient voltage and current during the switching process, $E = \int_0^t V(t)I(t)dt$.

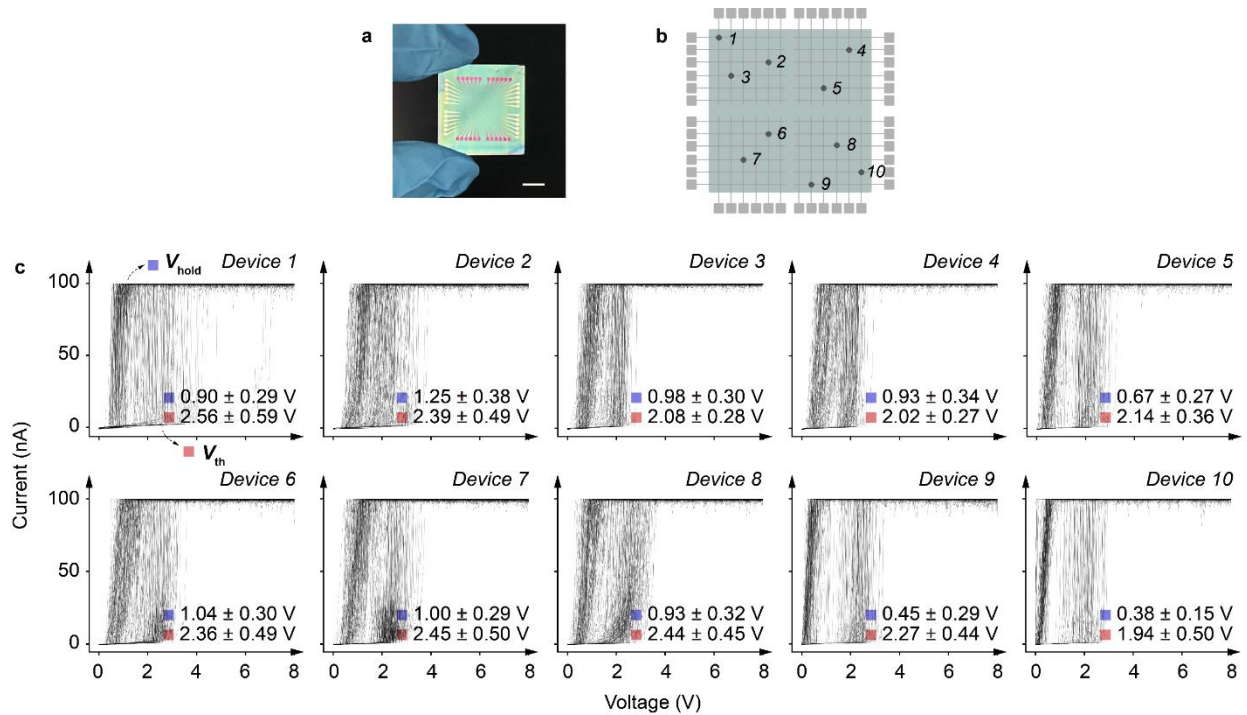


Figure S3. Device-to-device stochasticity. (a) 12×12 memristor array in a crossbar configuration, with a fabrication yield approximating 100% (replotted from Fig. 1a), and (b) the corresponding schematic array showing the devices randomly selected for the sampling test. Scale bar – 5 mm. (c) Current-voltage outputs from the randomly selected sampling memristor devices, showing 128-cycle stochastic yet stable switching with a ratio of $\sim 10^5$ for all the tested devices. A compliance current of 100 nA is set. V_{hold} and V_{th} denote the hold voltage and threshold voltage, respectively.

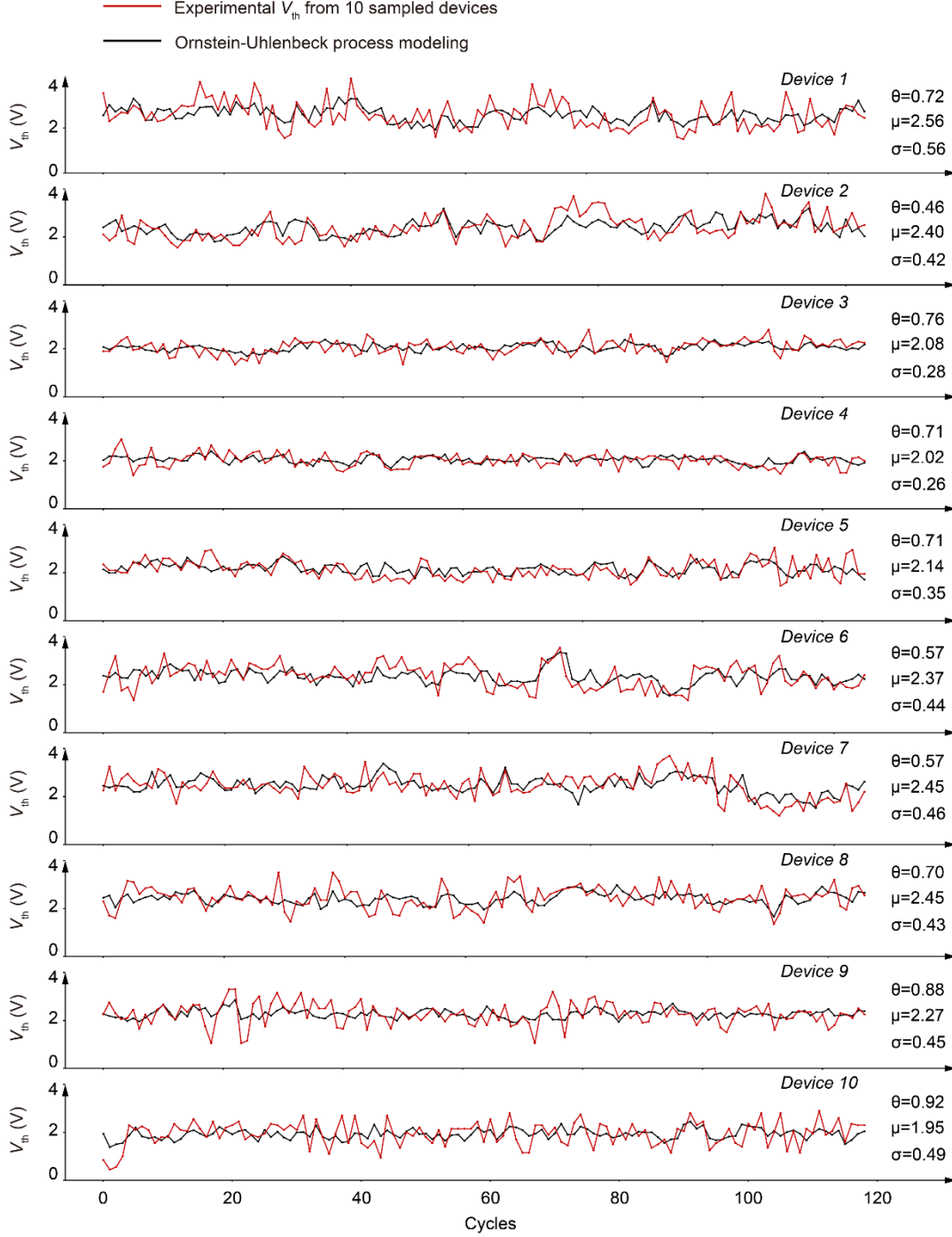


Figure S4. Stability test of the switching stochasticity from the randomly selected sampling memristor devices. Ornstein-Uhlenbeck process modeling on the measured threshold voltage V_{th} data points of the 10 sampled memristors across the 128 consecutive sweeping cycles present in Fig. 3c. The experimental V_{th} data points well fit an Ornstein-Uhlenbeck process, $dV_{th,t} = \theta(\mu - V_{th,t}) + \sigma dW_t$, where θ determines the magnitude of mean reversion, μ represents the asymptotic mean, σ stands for the variation, and dW_t denotes the variation of a Wiener process. The Ornstein-Uhlenbeck process describes a stochastic process in a dynamical system (3). This proves the stability of the memristor switching stochasticity in prolonged switching operations.

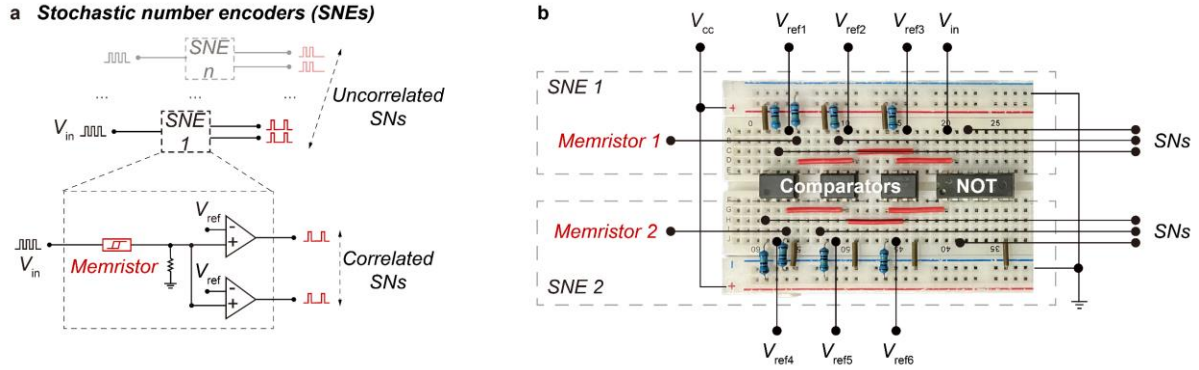
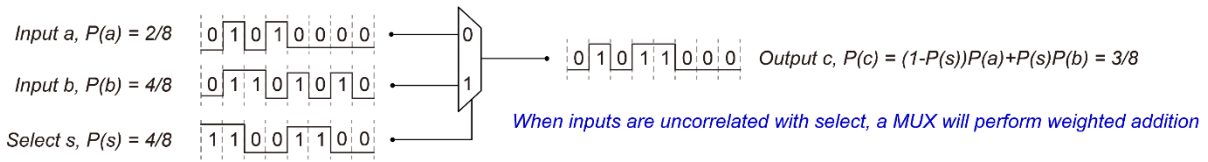


Figure S5. Stochastic number encoder. (a) Circuit design (replotted from Fig. 2a) and (b) the experimental setup of stochastic number encoders (SNEs). To build the SNEs, the memristors are tested on a probe station and connected to the logic gates and other electronic components on a breadboard. The electronic components include the comparators and resistors, as well as the NOT gates (connected to the output of comparators if negative correlation is required). Note that the voltage supply of the NOT gates is synchronized with V_{in} to the memristors to avoid output during the pulse intervals.

a Example - when select s is uncorrelated with inputs a and b



b Counter example - when select s is correlated with input a and/or b

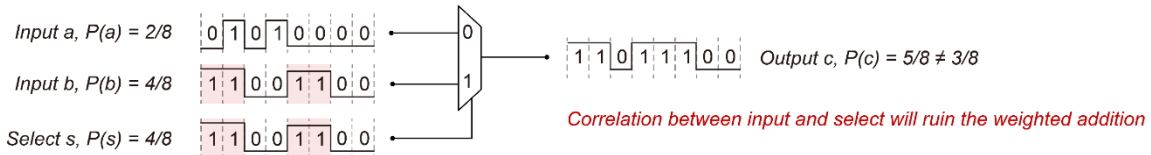
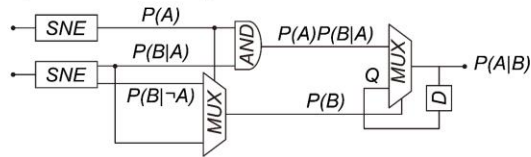


Figure S6. Probabilistic MUX logic. (a) An example showing the probabilistic MUX logic as a weighted Adder. In this case, the select s is uncorrelated with the inputs a and b . In contrast, the counter example of probabilistic MUX logic in (b) no longer performs weighted addition when the select s is correlated with the inputs a and/or b . A positive correlation between input b and select s corrupts the weighted addition operation, as s completely accepts b as part of the output c instead of selecting bits from b with a probability.

Bayesian inference theorem:

$$P(A|B) = \frac{P(A)P(B|A)}{P(B)} = \frac{P(A)P(B|A)}{P(A)P(B|A)+P(\neg A)P(B|\neg A)}$$

Operator circuit design:



Hardware implementation:

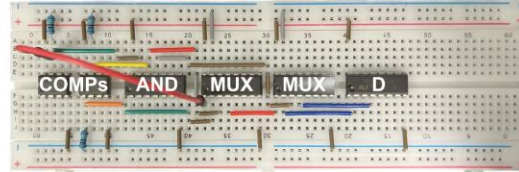


Figure S7. Bayesian inference operator. To realize the Bayesian inference theorem (same as that in Fig. 3a), the operator circuit consists of probabilistic AND and MUX logics. They are used to conduct multiplication and weighted addition operations, respectively, for functioning as the numerator and denominator of the Bayesian inference theorem. Probabilistic MUX plus a D-Flip-Flop is used to conduct division, designed following a classic divider design for stochastic numbers, named CORDIV (4). During the hardware tests, the memristors (not depicted here for the clarity of the circuit) are tested on a probe station and connected to the logic gates and other electronic components on the breadboard. The electronic components include the comparators (COMPs), D-Flip-Flop, and resistors. The comparator reference, voltage supply, and pulsed voltage signal inputs are powered by the arbitrary waveform generators (also not depicted here for clarity).

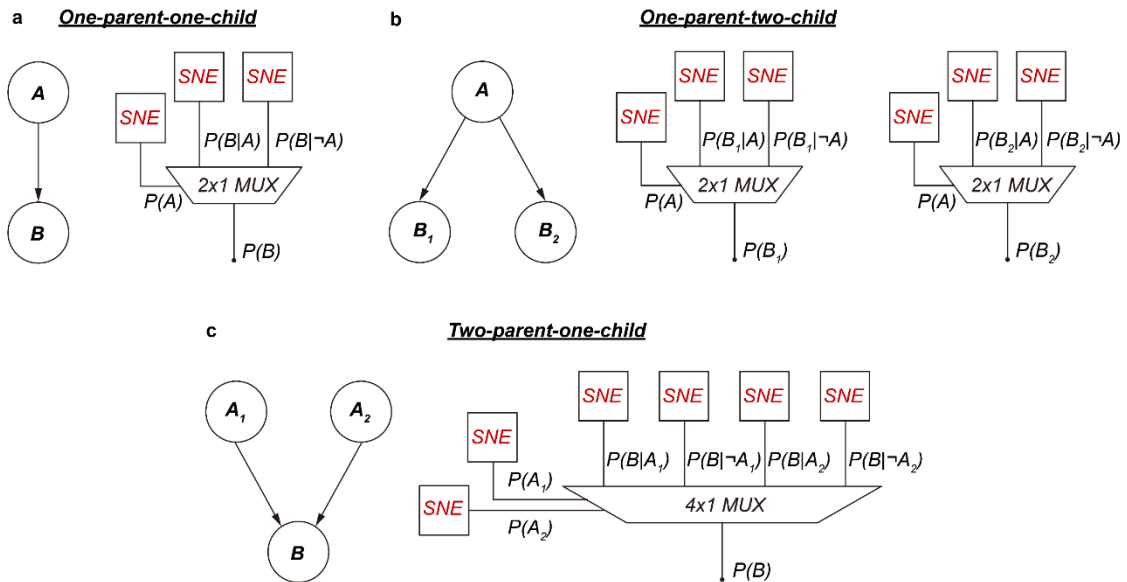
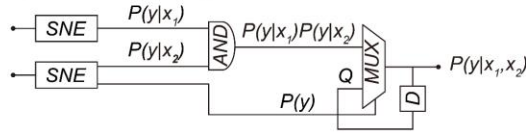


Figure S8. Basic dependencies within Bayesian inference and corresponding circuit design in probabilistic computing. Specifically, a 2×1 probabilistic MUX logic can be used in the one-parent-one-child case (a); a 4×1 probabilistic MUX logic can be used in the two-parent-one-child case (b); and two 2×1 probabilistic MUX logics can be used in the one-parent-two-child case (c).

Bayesian fusion theorem:

$$P(y|x_1, x_2) = \frac{P(x_1, x_2|y)P(y)}{P(x_1, x_2)} \propto \frac{P(y|x_1)P(y|x_2)}{P(y)}$$

Operator circuit design:



Hardware implementation:

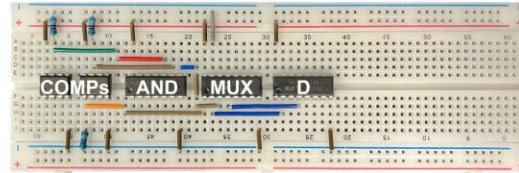


Figure S9. Bayesian fusion operator. To realize the Bayesian fusion theorem (same as that in Fig. 4a), the operator circuit consists of probabilistic AND and MUX logics. Probabilistic AND is used to conduct multiplication for functioning as the numerator of the Bayesian fusion theorem. Probabilistic MUX plus a D-Flip-Flop is used to conduct division, designed following a classic divider design for stochastic numbers, named CORDIV (4). During the hardware tests, the memristors (not depicted here for the clarity of the circuit) are tested on a probe station and connected to the logic gates and other electronic components on the breadboard. The electronic components include the comparators (COMPs), D-Flip-Flop, and resistors. The comparator reference, voltage supply, and pulsed voltage signal inputs are powered by the arbitrary waveform generators (also not depicted here for clarity).

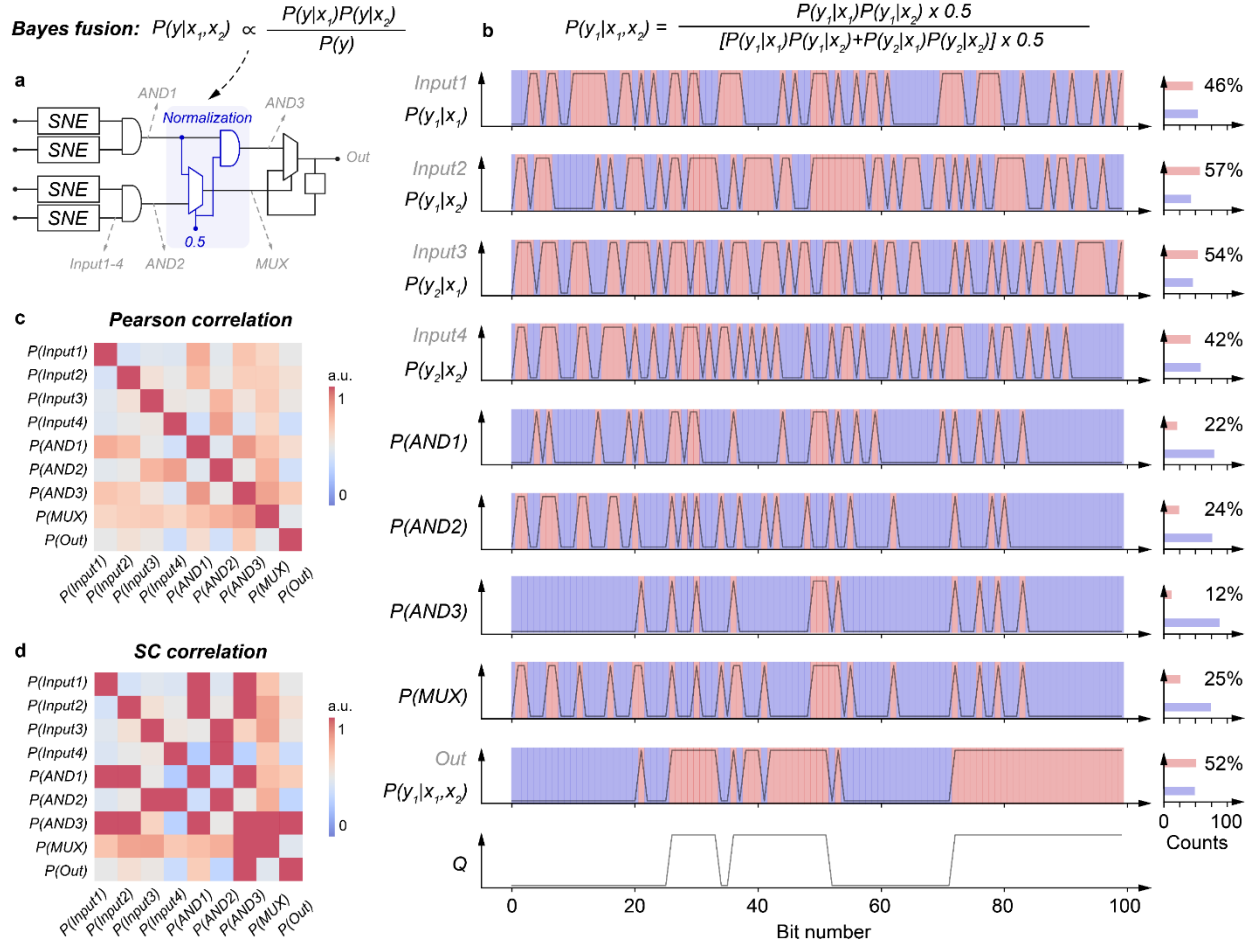


Figure S10. Bayesian fusion operator with a normalization module. (a) Circuit design of a Bayesian fusion operator. Probabilistic AND and MUX logics are used to conduct multiplication and weighted addition operations respectively for functioning as the numerator and denominator for the Bayesian fusion theorem. Probabilistic MUX plus a D-Flip-Flop is used to conduct division, designed following a classic divider design for stochastic numbers, named CORDIV (4). Additionally, a normalization module is integrated. (b) Simulation result of Bayesian fusion using the normalization module. The stochastic numbers at the key nodes in (a) are plotted. Bit 0s and 1s are marked in blue and red. Pairwise (c) Pearson and (d) SC correlations between stochastic numbers in (b).

Table S1. Probabilistic logic operations in varying correlation conditions. Probabilistic AND, OR, XOR, and MUX logics in the uncorrelated, positive correlated, and negative correlated cases are presented. The stochastic numbers are assumed in a unipolar format (5).

	Uncorrelated	Positively correlated	Negatively correlated
AND	$P(c) = P(a)P(b)$	$P(c) = \min(P(a), P(b))$	$P(c) = \max(P(a) + P(b) - 1, 0)$
OR	$P(c) = P(a) + P(b) - P(a)P(b)$	$P(c) = \max(P(a), P(b))$	$P(c) = \min(1, P(a) + P(b))$
XOR	$P(c) = P(a) + P(b) - 2P(a)P(b)$	$P(c) = P(a) - P(b) $	$P(c) = P(a) + P(b)$, if $P(a) + P(b) \leq 1$; $P(c) = 2 - (P(a) + P(b))$, otherwise.
MUX	$P(c) = (1 - P(s))P(a) + P(s)P(b)$, if s is uncorrelated with a and b		

Supplementary References

1. L. Song, P. Liu, J. Pei, F. Bai, Y. Liu, S. Liu, Y. Wen, L. W. T. Ng, K. P. Pun, S. Gao, M. Q. H. Meng, T. Hasan, G. Hu, Spiking neurons with neural dynamics implemented using stochastic memristors. *Adv. Electron. Mater.* **2300564**, 1–9 (2023).
2. S. S. Teja Nibhanupudi, A. Roy, D. Veksler, M. Coupin, K. C. Matthews, M. Disiena, Ansh, J. V. Singh, I. R. Gearba-Dolocan, J. Warner, J. P. Kulkarni, G. Bersuker, S. K. Banerjee, Ultra-fast switching memristors based on two-dimensional materials. *Nat. Commun.* **15** (2024).
3. S. Dutta, G. Detorakis, A. Khanna, B. Grisafe, E. Neftci, S. Datta, Neural sampling machine with stochastic synapse allows brain-like learning and inference. *Nat. Commun.* **13**, 2571 (2022).
4. T. H. Chen, J. P. Hayes, Design of division circuits for stochastic computing. *Proc. IEEE Comput. Soc. Annu. Symp. VLSI ISVLSI 2016-Septe*, 116–121 (2016).
5. A. Alaghi, W. Qian, J. P. Hayes, The promise and challenge of stochastic computing. *IEEE Trans. Comput.-Aided Des. Integr. Circuits Syst.* **37**, 1515–1531 (2018).